Structure of hydrated and sulfated stannous acid. Quantum chemical modeling

T. S. Zyubina[a, *], A.S . Zyubin[a], R. V. Pisarev[a], A. V. Pisareva[a], Yu. A. Dobrovolsky[a, b]

[a]*Federal Research Center of Problems of Chemical Physics RAS, Chernogolovka, 142432 Russia*

[b]*Center of Hydrogen Energy (PJSFC "Sistema"), Chernogolovka, 142432 Russian*

**e-mail:zyubin@icp.ac.ru*

Received August 17, 2024
Revised October 14, 2024
Accepted October 14, 2024

Different complexes of H_2SnO_3 and their hydrated and sulfated derivatives have been studied by quantum-chemical methods within the cluster approximation with the ωB97XD functional and LanL2DZ(Sn) and 6-31G**(O,S,H) basis sets, as well as considering periodic boundary conditions with the PBE functional and the PAW projected plane wave basis set. It has been established that among the hydrated forms, the smallest clusters with signs of SnO_2 crystal (2-3 times coordinated oxygen atoms and 5-6 times coordinated tin atoms) are clusters $(H_2SnO_3)_6$ with a circumscribed sphere diameter d ~10Å. Their merger (in the form of globules (d ~20Å), chains, films) is energetically favorable due to hydrogen bonds with each other and water molecules. Their enlargement is also possible due to Sn–O–Sn and Sn–OH–Sn covalent bonds with the formation of various larger nanoparticles, for example $(H_2SnO_3)_{12}$. Interestingly, some of them are hollow structures. Sulfuric acid molecules adsorbed on the surface of clusters $(SnO_2)_n(H_2O)_m$ are bound to the surface Sn atoms by SO_4^{2-} anions, and the protons released during this process complete the conduction channels, forming H_3O^+ and $H_5O_2^+$ cations in addition to OH^- anions and water.

Keywords: quantum-chemical modeling, density functional, stannic acid, proton exchange membranes

DOI: 10.31857/S0044457X250109e3

INTRODUCTION

Hydrated tin dioxide is used as a selective catalyst in oxidative dehydrogenation reactions of organic substances [1]. Gel-like hydrated dioxides of group IV elements are also used as adsorbents for the extraction of platinum group metals, gold, mercury, and copper from complexing media [2]. Recently, tin oxides have been most widely used in proton exchange (proton-conducting) membranes (**PEM**) for chemical power sources: in lithium-ion batteries and low-temperature fuel

cells. One way to improve the properties of PEMs is to include nanosized SnO_2 powders with surface functionalization in their composition, primarily with sulfuric acid and water. Papers [3-6] show the positive effect of introducing proton-conducting fillers such as hydrated tin oxide ($SnO_2 / n\ H_2O$) and its sulfated derivatives ($(SnO_2)_n(H_2SO_4)_k(H_2O)_m$, in some works abbreviated as $SSnO_2$) into membranes. Changes in surface morphology and improved hydration are reflected in increased proton conductivity of such composite membranes and their ability to operate in fuel cells under more severe conditions. In this regard, studying the reasons for such effective performance of nanostructures with composition $(SnO_2)_n(H_2SO_4)_k(H_2O)_m$ is of significant interest.

The hydrate $SnO_2 / n\ H_2O$ (α-stannic acid), soluble in acids and alkalis, is formed as a precipitate, for example, during the hydrolysis of $SnCl_4$ in the presence of NH_3. Over time or when heated, it transforms into β-stannic acid, which is soluble only in molten alkalis. It can be assumed that the decrease in the reactivity of β-stannic acid is associated with polycondensation processes, a decrease in the number of active OH groups, and the formation of strong Sn–O–Sn bonds.

Studies using the Mössbauer effect and X-ray diffraction lead to the conclusion about the cluster structure of stannic acids [7-9]. Stannic acid is highly dispersed and consists of particles characterized by an average X-ray diameter $d \approx 20$Å. However, analysis of the change in the Debye-Waller factor with changes in annealing temperature showed a significant proportion of smaller particles with a diameter of $d \leq 10$Å in stannic acid samples, the presence of which is not directly detected by X-ray diffraction. The shape of the resonance lines indicates that the immediate environment of tin atoms does not change during the transformations of stannic acids and corresponds to an octahedron of oxygen atoms.

Depending on the method of preparation and solubility, six varieties of stannic acids have been identified [10-12]. For example, the xerogel of hydrated tin dioxide

with the composition $SnO_2/1.75H_2O$ consists of tin-oxygen-hydroxyl fragments and represents a polymeric particle, the structure of which is formed by ≡Sn–O–Sn≡, ≡Sn–O(H)–Sn≡, ≡Sn–O–H bonds and is permeated by hydrogen bonds, including those involving H_2O molecules, which are part of the surface and internal layers of the particle [13]. In the structure of stannic acid granules, no more than 1 mole of water molecules is retained due to hydrogen bonds. The xerogel is dehydrated in the temperature range of 50-890°C. When heated to 123°C, processes occur within individual granules: molecular water is removed, polycondensation of bridge groups ≡Sn–O(H)–Sn≡ takes place, and some water molecules transition from molecular to hydroxyl form. Above 123°C, water removal leads to polycondensation of tin-oxygen groups, resulting in the enlargement of granules. At temperatures >200°C, the structure of the granules is defined as cassiterite covered with a layer of tin oxyhydrate [14]. When heated to 600°C, the particle sizes of SnO_2/nH_2O increase from 20 to 130Å [7, 9, 13, 15].

Thus, the precipitate of stannic acid can be considered as a type of inorganic polymer. During its preparation, the first stage is the formation of unstable hydroxide $Sn(OH)_4$. The stage of transformation of hydroxide into stannic acid gel occurs very quickly, however, part of the hydroxide ions remains in the structure of $SnO_2/2H_2O$ gel [16]. According to [13], at the initial stage, the composition of the precipitate corresponds to $SnO_2/1.75H_2O$. When heated to 123°C, the water content decreases to 0.75 per SnO_2, with further calcination, cassiterite nanocrystals with a hydrated surface are formed. In study [17], the composition of stannic acid at room temperature corresponds to the ratio of $SnO_2/1.3H_2O$. Analysis of these samples showed the presence of terminal and bridging hydroxyl groups (Sn–OH and Sn–(OH)–Sn respectively). Based on these results, a model was proposed according to which the core of the colloidal particle consists of crystalline tin dioxide, and the surface layer consists of tin hydroxide.

The introduction of a strong inorganic acid into proton exchange membranes generates significant interest due to its dual function – improving water retention and creating additional acid sites [18, 19]. The study [20] showed that on the surface of sulfated tin dioxide, Lewis acid sites in the presence of water can easily transform into Brønsted acid sites, which act as proton donors [19, 21]. In the composite membrane, acid sites and hydrophilic sulfonic acid groups on the surface of sulfated tin dioxide ($SSnO_2$) possess strong water-retaining properties. Moreover, $SSnO_2$ can provide additional sites for proton hopping from one ionic cluster to another, which can reduce resistance to proton transfer and increase the interaction of inorganic fillers with polymers [4, 5]. Reference [5] examined the effect of sulfation on the properties of SnO_2 nanoparticles incorporated into Nafion-based hybrid membranes. It was found that the amount of sulfate groups chemisorbed on the SnO_2 surface increases with decreasing oxide particle size. Smaller crystallite size and higher surface sulfation contribute to greater water affinity and more regular organization of ionic channels [5].

The purpose of this work is to study the structure of stannic acid clusters and their sulfated nanoparticles, to model proton-conducting channels in them, and to understand the nature of gel formation based on them.

METHODOLOGY

To evaluate the structure and stability of various formation variants of the studied systems, modeling was performed within the cluster approximation using the hybrid density functional ωB97XD [22] with 6-31G** basis sets for S, O, H atoms [23] and LanL2DZ for Sn with LanL2 pseudopotential [24,25] using the GAUSSIAN-09 software package [26]. For modeling polymeric systems (gel type), the periodic boundary conditions (**PBC**) approximation was used with the PBE functional [27] and projected augmented wave basis (PAW [28]) with energy cutoffs

of 400 and 600 eV within the VASP software package [29-32]. When determining the energy characteristics of the studied systems, their geometric parameters were fully optimized.

In this work, we have calculated clusters with sizes of the describing sphere d ≤20 Å and polymer strands, films, and globules formed from them. The repeating fragment used for calculation in the periodic boundary conditions approximation will be enclosed in square brackets in the text. For example, the repeating fragment of an infinite film $(SnO_2)_{12}(H_2SO_4)_{12}(H_2O)_4$ (with a ratio of $1SnO_2/1H_2SO_4/1.3H_2O$) is denoted as $[(SnO_2)_{12}(H_2SO_4)_{12}(H_2O)_4]$.

The structures and relative energies of the most typical nanoclusters are shown in Fig. 1, 2, and the energies of decomposition into fragments are given in Tables 1, 2. The adopted energy designations: E (SCF) (calculated within the self-consistent field framework) and E (H) (taking into account the enthalpy of formation at a temperature of 298.15 K and a pressure of 1 atm). The enthalpy was calculated in the rigid rotator-harmonic oscillator approximation; for this purpose, calculations of vibration frequencies were performed, the values of which are strictly positive for the given structures. Below, only the most energetically favorable configurations of the complexes will be considered.

Comparative characteristics of calculation levels. To compare the interaction energy of water molecules with the modeled systems and the hydrogen bond energy between water molecules within the used approximation (ωB97XD), a calculation of a cluster of 12 water molecules was performed. Within this model, the energy of each hydrogen bond in the cluster was 0.3 eV(H), which is in good agreement with the experimental estimate of this value (0.3 eV [33]).

Relative energies (E) obtained within the self-consistent field (SCF) framework and taking into account enthalpy (H) at a temperature of 298.15K and pressure of 1 atm are close (within 0.1 eV). The transition from the ωB97XD

functional with a Gaussian function basis to calculations at the PBE/PAW level reduces the formation energy values of nanostructures by 1-1.5 eV, while the trends in binding energy changes in the series are the same for these calculation levels. Modeling of polymer systems and films was performed using periodic boundary conditions and plane wave basis sets. Within this approximation, there are no edge effects or basis set superposition effects.

RESULTS AND DISCUSSION

Hydrated tin oxide $(SnO_2)_n(H_2O)_m$

The calculated structures of clusters $(SnO_2)_n(H_2O)_m$ (in some cases from two angles) are shown in Fig. 1 (relative energies of isomers are given after the comma in eV), in some cases hydrogen bonds are shown with dotted lines. Since H_2SnO_3 molecules (ratio $1SnO_2/1H_2O$) contain two OH fragments and a double O=Sn bond, they combine with a significant decrease in total energy, forming oligomers and polymers. Already when combining into a dimer (Table 1, Fig. 1), the energy gain exceeds 2 eV for each H_2SnO_3 fragment. As the number of combined H_2SnO_3 molecules increases, the magnitude of energy reduction increases and reaches saturation, therefore, up to certain sizes, it is energetically favorable to combine into larger particles. With a small number of H_2SnO_3 fragments, cyclic structures of complexes are energetically more favorable than bulk ones, however, further small complexes begin to combine into bulk structures, for example, two molecules $(H_2SnO_3)_3$ combine into $(H_2SnO_3)_6$, and two $(H_2SnO_3)_6$ – into $(H_2SnO_3)_{12}$ and so on. At large values of n, water is displaced to the surface, and inside the complex, the area of the crystalline structure of SnO_2 grows, an example is structure **8** ($(SnO_2)_{32}(H_2O)_{44}$, Fig. 1).

The smallest clusters with crystal features (threefold coordinated oxygen atoms, five- and sixfold coordinated tin atoms) are, for example, clusters $(H_2SnO_3)_6$ (structure **3**) with a ratio of $1SnO_2/1H_2O$, $(H_2SnO_3)_6(H_2O)_2$ (structure **6**) with a ratio of $1SnO_2/1.3H_2O$ and $(H_2SnO_3)_6(H_2O)_4$ (structure **9**) with a ratio of $1SnO_2/1.7H_2O$ (d = 12–13 Å, Fig. 1), etc. The presence of a large number of terminal OH fragments and H_2O molecules leads to the possibility of these clusters sticking together. This results in extended structures, threads and films (for example, type **12** and **12a** for $(H_2SnO_3)_{24}(H_2O)_{16}$); globules (type **4** for $(H_2SnO_3)_{12}$ or **11** , **11a** for $(H_2SnO_3)_{12}(H_2O)_8$); hollow large clusters (**4a** , **4b**); chains connected by hydrogen bonds (type **11b** for $(H_2SnO_3)_{12}(H_2O)_8$), etc.

Interaction with water leads to undercoordinated tin atoms on the cluster surface completing their coordination to six. Thus, in isomer **6** ($(H_2SnO_3)_6(H_2O)_2$), the framework oxygen atoms and water molecules are triply coordinated, the two tin atoms bound to water are six-fold coordinated, the remaining four tin atoms are five-fold coordinated, and the terminal oxygen atoms bound to hydrogen atoms are doubly coordinated (ratio $1SnO_2/1.3H_2O$). When polymers form, it is possible to form both hydrogen-bonded complexes like structure **7d** ($(H_2SnO_3)_{12}(H_2O)_4$), and more energetically favorable covalently bonded clusters (via Sn–O(H)–Sn bridges) with structures **7** , **7a** – **7c** . The latter form because the OH groups on the cluster surface are shared between two adjacent tin atoms, making both of them six-fold coordinated. The structures $(H_2SnO_3)_{12}(H_2O)_8$ with a ratio of $1SnO_2/1.7H_2O$ behave similarly. Further addition of water leads to the formation of structure type **10** ($(H_2SnO_3)_6(H_2O)_6$) with a ratio of $1SnO_2/2H_2O$, where all tin atoms are six-fold coordinated, so covalently bonded polymers of the type described above should not be expected (however, this does not negate the possibility of combining to form larger structures with water elimination).

The presence of the structures described above may lead to the introduction of hydrated tin oxide (SnO_2/nH_2O) having a positive effect on membrane properties [4, 5]. The obtained data are in good agreement with studies using the Mössbauer effect and X-ray diffraction, and with conclusions about the cluster and highly dispersed structure of stannic acids with an average X-ray particle diameter from 10 to 20Å, and with the fact that the nearest environment of tin atoms does not change during the transformations of stannic acids and corresponds to an octahedron of oxygen atoms [7–9, 13, 14].

The binding energy value of stannic acid with water molecules (calculated per one water molecule as $E_B = \{E(A) + mE(B) - E[AB_m\}/m$, where $E(A)$, $E(B)$ and $E[AB_m]$ are the energies of the cluster $(SnO_2)_n$, water molecule and cluster $(SnO_2)_n(H_2O)_m$ respectively) is greater than the energy of the hydrogen bond between water molecules. Therefore, they attach to the stannic acid clusters with energies of 1.4–2.0 eV (Table 1, Fig. 1), forming proton-conducting channels. However, in the case of $(SnO_2)_n(H_2O)_m$ these channels are chaotic in nature (Fig. 1).

Sulfated Tin Hydroxide $(SnO_2)_n(H_2SO_4)_k(H_2O)_m$

The structure of complexes $(SnO_2)_n(H_2O)_k(H_2SO_4)_m$ (Table 2, Fig. 2) has significant similarity with the structure of the analogous hydroxides $(SnO_2)_n(H_2O)_m$ considered above. However, the formation of the molecule $(SnO_2)_n(H_2SO_4)_k(H_2O)_m$ from SnO_2, H_2SO_4 and H_2O proceeds with a more significant energy decrease (Table 2), while the addition of H_2SO_4 to the stannic acid hydrate cluster is energetically one and a half to two times more favorable than adding a water molecule to the sulfate of this cluster (Tables 1 and 2).

For example, the addition of six H_2SO_4 molecules to structure **13**, in which SO_4^{2-} anions attach with two oxygen atoms to the tin atoms of the surface, and

the acid protons combine with OH fragments, forming six H_3O^+ cations that are part of the proton-conducting layer. On the cluster surface, negatively ($Q(SO_4) = -1.3\ e$) and positively ($Q(H_3O) = 0.7\ e$) charged (according to Mulliken) fragments alternate. The diameter of the describing sphere increases from 10 (**3**) to 12 Å (**13**) during sulfation.

Molecules of sulfuric acid can attach to the surface of hydrated clusters based on SnO_2 in two ways: 1) by integrating into the hydrogen bond system of the surface layer and partially retaining their structure, for example structure **15a** $((H_2SnO_3)_6(H_2SO_4)_6(H_2O)_2)$, and 2) by displacing some water molecules from the SnO_2 surface and forming SO_4^{2-} anions bound to tin atoms, i.e., sulfuric acid molecules displace water molecules to the outer sphere, for example structure **15** $((H_2SnO_3)_6(H_2SO_4)_6(H_2O)_2)$, Fig. 2. The first method is energetically less favorable. As the number of adsorbed sulfuric acid molecules increases, the interaction between them significantly affects the system's energy. When the cluster surface is completely covered with sulfuric acid molecules, a layer is formed consisting of SO_4^{2-} anions bound to tin atoms, Sn–O–Sn bridges, and a proton-conducting layer consisting of water, OH^+ and H_3O^+ (see, for example, $(H_2SnO_3)_{12}(H_2SO_4)_{12}(H_2O)_4$ (structure **18** , Fig. 2)). Sulfated nanoclusters of stannic acid form more ordered proton-conducting channels compared to hydrated ones. For example, in Fig. 2, structure **18** $((H_2SnO_3)_{12}(H_2SO_4)_{12}(H_2O)_4)$ with a ratio of $1SnO_2/1H_2SO_4/1.3H_2O$ clearly shows proton-conducting channels, while in Fig. 1 for a similar hydrate $(H_2SnO_3)_{12}(H_2O)_4$ (structure **7**) with the same ratio $1SnO_2/1.3H_2O$, only scattered disordered hydrogen bonds are visible. Sulfation led to the formation of 12 H_3O^+ cations, which connected the proton-conducting channels to each other, while the presence of 12 SO_4^{2-} fragments ordered them.

Polymerization

The presence of a large number of fragments forming hydrogen bonds leads to gelation. For example, the structures $[(H_2SnO_3)_{12}(H_2SO_4)_{12}(H_2O)_4]$ form threads and films like structures **19** and **20** , shown in Fig. 3, due to hydrogen bonds. The infinite conduction channels formed in them are similar to those considered above for the cluster $(H_2SnO_3)_{12}(H_2SO_4)_{12}(H_2O)_4$(structure **18** , Fig. 2).

CONCLUSION

Based on the obtained data, it can be expected that during the deposition of stannic acid from solution through self-assembly, hydrated structures based on $SnO_2 \cdot n H_2O$ clusters with a quasi-crystalline core may form. During their sulfation, it is possible to obtain complexes in which SO_4^{2-} anions are attached to tin atoms through two oxygen atoms, and the separated protons, binding with oxygen atoms of OH fragments and water, form a proton-conducting layer that is more ordered and has many more H_3O^+ cations compared to non-sulfated structures. This may explain the increase in conductivity during sulfation noted in works [13, 17]. As a result of the formation of a well-structured proton-conducting layer on the surface of clusters, sulfated tin hydroxide ($SSnO_2$) can provide additional sites for proton hopping from one ionic cluster to another, which may lead to a decrease in resistance to proton transfer, as well as an increase in interaction between polymers [20, 21]. Since sulfate groups are located on the surface of oxide clusters, the relative amount of sulfate groups chemisorbed on the surface increases with decreasing particle size (but not more than $1SnO_2/1H_2SO_4$). Smaller crystallite size and higher surface sulfation contribute to a more regular organization of ionic channels, which is consistent with experimental results [4, 20].

In sulfated structures $(SnO_2)_n(H_2SO_4)_k(H_2O)_m$, proton-conducting channels are formed, while for a similar hydrate with the same composition $(SnO_2)_n(H_2O)_m$

, only scattered disordered hydrogen bonds are visible. Sulfation leads to the formation of H_3O^+ cations that connect the proton-conducting layers to each other, and the presence of SO_4^{2-} fragments orders the conducting channels.

Of course, the results obtained in this work do not claim to provide a quantitative description of the relative stability of various formations consisting of tin dioxide, water and sulfuric acid when their structure and composition change, however, based on previous calculations of this level, one can expect that they correctly describe relative changes and qualitative picture.

The obtained data are in good agreement with the results obtained in the study of catalytic reactions of oligomerization and isomerization of sulfated SnO_2-based systems [34, 35] and proton conductivity of hydrated SnO_2 [36, 37].

FUNDING

The work was carried out in accordance with the state assignment (topic No. 124013000692-4) at the Computing Center of FRC ChPh and MC RAS. Part of the calculations was performed on the GODWIN workstation at the D.S. Korzhinskii Institute of Experimental Mineralogy in Chernogolovka.

CONFLICT OF INTEREST

The authors declare that they have no conflict of interest.

REFERENCES

1. *Hattori T., Athoh S., Tagawa T., Murakami J.* Preparation of Catalysts IV. Amsterdam: Elsevier, 1987. p. 113. https://shop.elsevier.com/books/preparation-of-catalysts-iv/poncelet/978-0-444-42796-0
2. Pechenyuk S.I. // Russ. Chem. Bull. 1999. V. 48. P. 229. https://link.springer.com/article/10.1007/BF02494538
3. *Kesava M., Dinakaran K* . // J. Phys. Chem. C. 2021. V. 125. P. 130. https://dx.doi.org/10.1021/acs.jpcc.0c08739
4. *Scipioni R., Gazzoli D., Teocoli F. et al.* // Membranes. 2014. V. 4. P. 123. https://www.mdpi.com/2077-0375/4/1/123

5. *Chen F., Mecheri B., D'Epifanio A. et al* . // Fuel Cells. 2010. V. 10. № 5. P. 790. https://onlinelibrary.wiley.com/doi/abs/10.1002/fuce.200900179
6. *Brutti S., Scipioni R., Navarra M.A. et al.* // Int. J. Nanotechnol. 2014. V. 11. P. 882. https://www.inderscienceonline.com/doi/abs/10.1504/IJNT.2014.063796
7. *Fabrichnyi P.B., Babeshkin A.M., Portyanoi V.A. et al* . // J. Struct. Chem. 1970. No. 4. P. 772.
8. *Fabrichnyi P.B., Babeshkin A.M., Portyanoi V.A. et al.* // J. Struct. Chem. 1971. V. 11. P. 715. https://link.springer.com/article/10.1007/BF00743453
9. *Fabrichnyi P.B., Babeshkin A.M., Nesmeyanov A.N.* // J. Phys. Chem. Solids. 1970. V. 31. P. 1399. https://www.sciencedirect.com/science/article/abs/pii/0022369770901447
10. *Willstuter R., Krant H., Fremery R.* // Ber. 1924. Bd. 57. S. 1491.
11. *Denisova E.F., Pletnev R.N., Fedotov M.A. et al.* Solid State Radio Spectroscopy. Sverdlovsk: USC AS USSR, 1984. P. 54.
12. *FabritchnyiP., AfanassovM., DemazeauG.* // C.R. Acad. Sc. Paris. 1986. V. 303. Ser. II. P. 1197.
13. *Kostrikin A.V., Spiridonov F.M., Linko I.V. et al.* // J. Struct. Chem. 2007. V. 52. P. 1176. *Kostrikin A.V., Spiridonov F.M., Lin'ko I.V. et al.* // Russ. J. Inorg. Chem. 2007. V. 52. P. 1098. https://link.springer.com/article/10.1134/S0036023607070182
14. *Giesekke E.W., Gutowsky H.S., Kirkov P. et al.* // Inorg. Chem. 1967. V. 6. P. 1294. https://pubs.acs.org/doi/10.1021/ic50053a005
15. *Parshutkin V.V., Yaroslavtsev A.B., Prozorovskaya Z.N. et al.* // Russ. J. Inorg. Chem. 1985. V. 30. No. 1. P. 56.
16. *Brauer G.* Handbook der Preparativen Anorganischen Chemie in drei Banden. Stuttgart: Ferdinand Enke Verlag, 1975.
17. *Karelin A.I., Leonova L.S., Tkacheva N.S. et al.* // Heliyon. 2022. V. 8. P. e11450. https://doi.org/10.1016/j.heliyon.2022.e11450
18. *Liu L., Pu Y., Lu Y. et al.* // J. Membr. Sci. 2021. V. 621. P. 118972. https://doi.org/10.1016/j.memsci.2020.118972
19. *Navarra M.A., Abbati C., Scrosati B.* // J. Power Sources. 2008. V. 183. P. 109. https://doi.org/10.1016/j.jpowsour.2008.04.033
20. *Arata K.* // Green Chem. 2009. V. 11. P. 1719. https://doi.org/10.1039/B822795K
21. *Varala R., Narayana V., Kulakarni S.R. et al.* // Arab. J. Chem. 2016. V. 9. P. 550. https://www.sciencedirect.com/science/article/pii/S1878535216300028
22. *Chai J.-D., Head-Gordon M.* // J. Chem. Phys. 2008. V. 128. P. 084106. https://doi.org/10.1063/1.2834918
23. *Krishnan R., Binkley J.S., Seeger R. et al.* // J. Chem. Phys. 1980. V. 72. P. 650. https://doi.org/10.1063/1.438955
24. *Johnson B.J., Gill P.M.W., Pople J.A.* // J. Chem. Phys. 1993. V.98. P. 5612. https://doi.org/10.1063/1.464906
25. *Wadt W.R., Hay P.J.* // J. Chem. Phys. 1985. V. 82. P. 284. https://doi.org/10.1063/1.448800
26. *Frisch M.J., Trucks G.W., Schlegel H.B. et al.* Gaussian 09, Revision B.01, Gaussian, Inc., Wallingford CT, 2010.
27. *Perdew J.P., Burke K., Ernzerhof M.* // Phys. Rev. Lett. 1996. V. 77. P. 3865. https://doi.org/10.1103/PhysRevLett.77.3865
28. *Hafner J.* // J. Comput. Chem. 2008. V.29. P. 2044. https://doi.org/10.1002/jcc.21057

29. *Kresse G., Hafner J.* // Phys. Rev. B. 1993. V. 47. P. 558. https:// doi.org /10.1103/PhysRevB.47.558
30. *Kresse G., Hafner J.* // Phys. Rev. B. 1994. V.49. P. 14251.
31. *Kresse G., Furthmuller J.* // Phys. Rev. B. 1996. V. 54. P. 11169. https://doi.org/10.1103/physrevb.54.11169
32. *Kresse G., Joubert D.* // Phys. Rev. B. 1999. V. 59. P. 1758. https://doi.org/10.1103/physrevb.59.1758
33. *Huheey J.* Inorganic Chemistry. Moscow: Khimiya, 1987. 695 p.
34. Straumal E.A., Yurkova L.L., Baranchikov A.E. et al. // Russ. J. Inorg. Chem. 2021. V. 66. P. 288. https://link.springer.com/article/10.1134/S0036023621020194
35. LermontovS.A., YurkovaL.L., StraumalE.A. etal. // Russ. J. Inorg. Chem. 2018. V. 63. P. 303.https://link.springer.com/article/10.1134/S0036023618030142
36. Karelin A.I., Tkacheva N.S., Nadkhina S.E. et al. // Russ. J. Inorg. Chem. 2016. V. 61. P. 1144.https://link.springer.com/article/10.1134/S0036023616090084
37. Karelin A.I., Leonova L.S., Arsatov A.V. et al. // Russ. J. Inorg. Chem. 2013. V. 58. P. 711.https://link.springer.com/article/10.1134/S0036023613060120

Table 1. Formation energies of clusters $(SnO_2)_n(H_2O)_m$, eV

$(SnO_2)_n(H_2O)_m$	SCF	*H*
$H_2O+SnO_2 \rightarrow (H_2SnO_3)$ (**1**)	2.5	2.4
$2(H_2SnO_3)$ (**1**) $\rightarrow (H_2SnO_3)_2$	2.8 × 2	2.8 × 2
$3(H_2SnO_3)$ (**1**) $\rightarrow (H_2SnO_3)_3$ (**2**)	3.5 × 3	3.4 × 3
$4(H_2SnO_3)$ (**1**) $\rightarrow (H_2SnO_3)_4$	3.7 × 4	3.6 × 4
$5(H_2SnO_3)$ (**1**) $\rightarrow (H_2SnO_3)_5$	4.1 × 5	4.0 × 5
$6(H_2SnO_3)$ (**1**) $\rightarrow (H_2SnO_3)_6$ (**3**)	4.2 × 6	4.2 × 6
$12(H_2SnO_3)$ (**1**) $\rightarrow (H_2SnO_3)_{12}$ (**4**)	4.9 × 12	4.8 × 12
$16(H_2SnO_3)$ (**1**) $\rightarrow (H_2SnO_3)_{16}$	5.0 × 16	4.9 × 16
$2(H_2SnO_3)_3$ (**2**) $\rightarrow (H_2SnO_3)_6$ (**3**)	2.4 × 2	2.3 × 2
$2(H_2SnO_3)_6$ (**3**) $\rightarrow (H_2SnO_3)_{12}$ (**4**)	4.0 × 2	3.9 × 2
$2(H_2SnO_3)_3(H_2O)_1$ (**5**) $\rightarrow (H_2SnO_3)_6(H_2O)_2$ (**6**)	2.4 × 2	2.3 × 2
$2(H_2SnO_3)_6(H_2O)_2$ (**6**) $\rightarrow (H_2SnO_3)_{12}(H_2O)_4$ (**7**)	4.7 × 2	4.6 × 2
$2(H_2SnO_3)_3(H_2O)_1$ (**5**) $\rightarrow (H_2SnO_3)_6(H_2O)_2$ (**6**)	2.1 × 2	2.1 × 2
$2(H_2SnO_3)_6(H_2O)_2$ (**6**) $\rightarrow (H_2SnO_3)_{12}(H_2O)_4$ (**7**)	2.6 × 2	2.6 × 2
$2(H_2SnO_3)_3(H_2O)_2 \rightarrow (H_2SnO_3)_6(H_2O)_4$ (**9**)	2.6 × 2	2.5 × 2
$2(H_2SnO_3)_6(H_2O)_4$ (**9**) $\rightarrow (H_2SnO_3)_{12}(H_2O)_8$ (**11**)	1.6 × 2	1.6 × 2
$2(H_2SnO_3)_{12}(H_2O)_8$ (**11**) $\rightarrow (H_2SnO_3)_{24}(H_2O)_{16}$ (**12**)	1.7 × 2	1.6 × 2
$(H_2SnO_3)+H_2O \rightarrow Sn(OH)_4$	3.3	3.3
$(H_2SnO_3)_2+H_2O \rightarrow (H_2SnO_3)_2H_2O$	1.4	1.4
$(H_2SnO_3)_3+H_2O \rightarrow (H_2SnO_3)_3H_2O$ (**5**)	1.5	1.4
$(H_2SnO_3)_3H_2O+H_2O \rightarrow (H_2SnO_3)_3(H_2O)_2$	1.0	0.9
$(H_2SnO_3)_6$ (**3**) $+H_2O \rightarrow (H_2SnO_3)_6H_2O$	1.4	1.3

$(H_2SnO_3)_6(H2O) + H_2O \rightarrow (H_2SnO_3)_6(H_2O)_2$ (**6**)	1.1	1.0
$(H_2SnO_3)_6(H_2O)_2 + 2H_2O \rightarrow (H_2SnO_3)_6(H_2O)_4$ (**7**)	1.4 × 2	1.4 × 2
$(H_2SnO_3)_6 + 2H_2O \rightarrow (H_2SnO_3)_6(H_2O)_2$ (**6**)	1.3 × 2	1.2 × 2
$(H_2SnO_3)_6 + 4H_2O \rightarrow (H_2SnO_3)_6(H_2O)_4$ (**7**)	1.4 × 4	1.3 × 4
$(H_2SnO_3)_6 + 6H_2O \rightarrow (H_2SnO_3)_6(H_2O)_6$	1.4 × 6	1.3 × 6
$(H_2SnO_3)_6 + 8H_2O \rightarrow (H_2SnO_3)_6(H_2O)_8$	1.2 × 8	1.1 × 8
$(H_2SnO_3)_{16} + 4H_2O \rightarrow (H_2SnO_3)_{16}(H_2O)_4$	1.7 × 4	1.7 × 4
$(SnO_2)_{32} + 44H_2O \rightarrow (SnO_2)_{32}(H_2O)_{44}$ (**8**)	2.0 × 44	2.0 × 44

Table 2. Formation energies of clusters $(SnO_2)_n(H_2SO_4)_k(H_2O)_m$

$(SnO_2)_n(H_2SO_4)_k(H_2O)_m$	SCF	*H*
$(H_2SO_4) + H_2O \rightarrow OS(OH)_4$	1.9	1.9
$(H_2SnO_3)_3H_2O + (H_2SO_4) \rightarrow (H_2SnO_3)_3(H_2SO_4)H_2O$	1.7	1.6
$(H_2SnO_3)_3(H_2SO_4) + H_2O \rightarrow (H_2SnO_3)_3(H_2SO_4)H_2O$	1.0	0.9
$(H_2SnO_3)_3(H_2SO_4)_2 + H_2O \rightarrow (H_2SnO_3)_3(H_2SO_4)_2H_2O$	1.1	1.0
$(H_2SnO_3)_3(H_2SO_4)_3 + H_2O \rightarrow (H_2SnO_3)_3(H_2SO_4)_3H_2O$ (**14**)	1.1	1.0
$(H_2SnO_3)_3 + (H_2SO_4) \rightarrow (H_2SnO_3)_3(H_2SO_4)$	2.2	2.1
$(H_2SnO_3)_3(H_2SO_4) + H_2SO_4 \rightarrow (H_2SnO_3)_3(H_2SO_4)_2$	2.1	2.0
$((H_2SnO_3)_3(H_2SO_4)_2 + H_2SO_4 \rightarrow H_2SnO_3)_3(H_2SO_4)_3$	2.4	2.2
$(H_2SnO_3)_6(H_2SO_4)_6$ (**13**) $+ 2H_2O \rightarrow (H_2SnO_3)_6(H_2SO_4)_6(H_2O)_2$ (**15**)	0.9 × 2	0.9 × 2
$(H_2SnO_3)_6(H_2SO_4)_6$ (**13**) $+ 6H_2O \rightarrow (H_2SnO_3)_6(H_2SO_4)_6(H_2O)_6$ (**13**)	0.8 × 6	0.8 × 2
$(H_2SnO_3)_6(H_2SO_4)_6$ (**13**) $+ 8H_2O \rightarrow (H_2SnO_3)_6(H_2SO_4)_6(H_2O)_8$ (**16**)	0.9 × 8	0.8 × 2
$(H_2SnO_3)_6(H_2SO_4)_6$ (**13**) $+ 14H_2O \rightarrow (H_2SnO_3)_6(H_2SO_4)_6(H_2O)_{14}$ (**17**)	0.9 × 14	0.8 × 2
$2(H_2SnO_3)_6(H_2SO_4)_6(H_2O)_2$ (**15**) $\rightarrow (H_2SnO_3)_{12}(H_2SO_4)_{12}(H_2O)_4$ (**18**)	1.2 × 2	1.2 × 2

FIGURE CAPTIONS

Fig. 1. Structures $(SnO_2)_n(H_2O)_m$. Relative energies of isomers are given after the comma (in eV).

Fig. 2. Structures $(SnO_2)_n(H_2SO_4)_k(H_2O)_m$ (shown from two angles in some cases). Relative energies are given after the comma (in eV). In some cases, hydrogen bonds are shown with dashed lines.

Fig. 3. Structures of thread and film $[(H_2SnO_3)_{12}(H_2SO_4)_{12}(H_2O)_4$. Hydrogen bonds are shown with dashed lines.

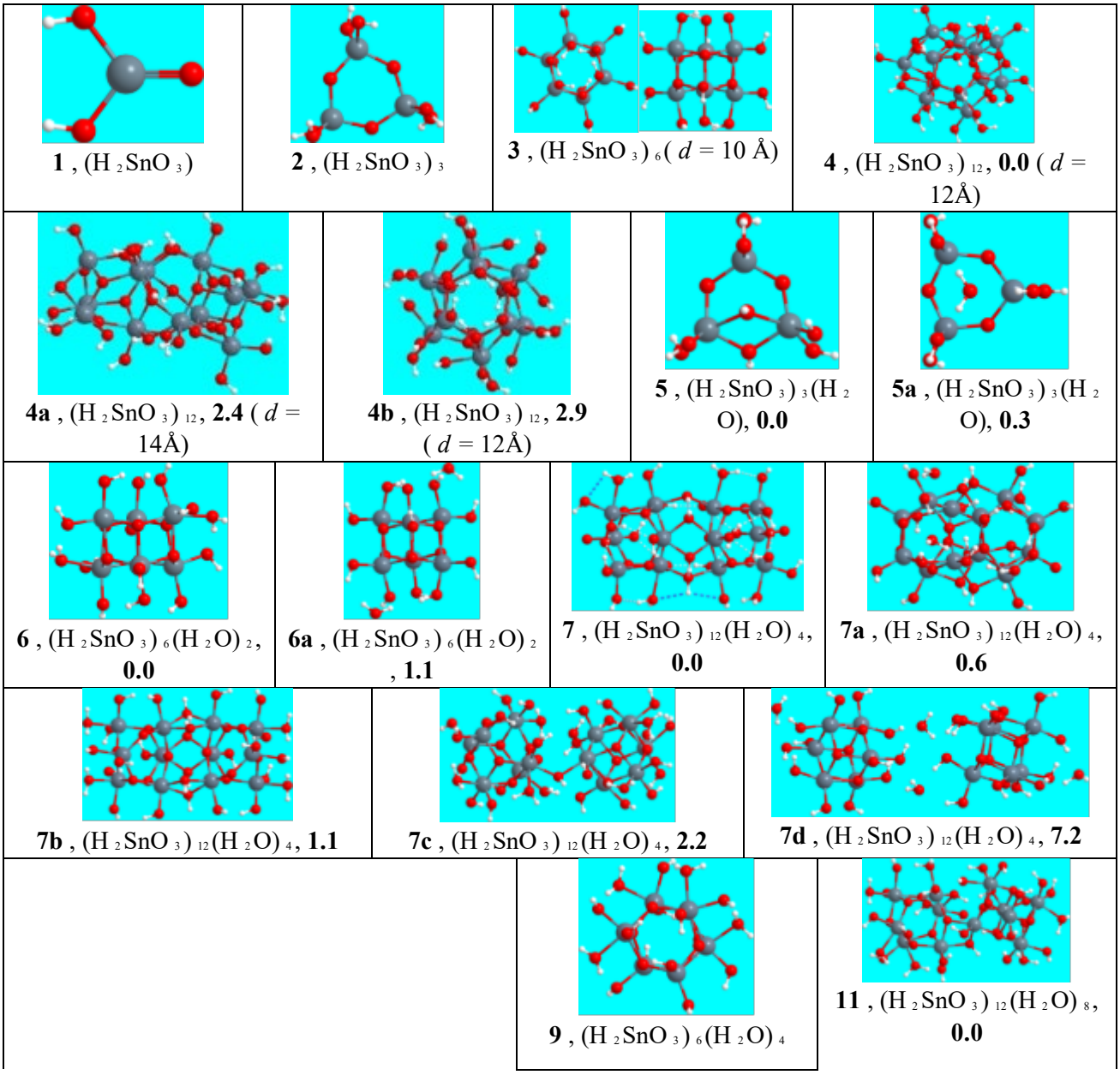

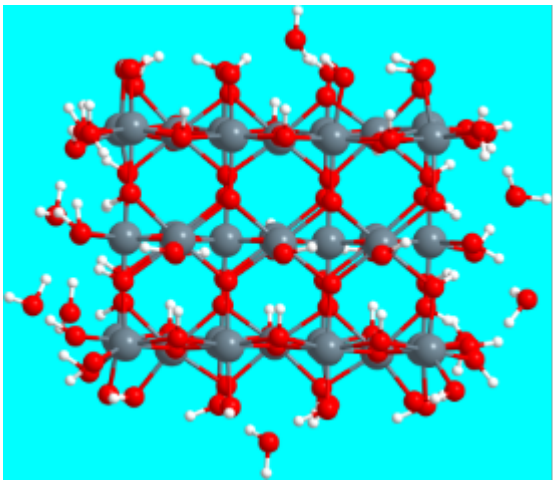

8 , $(SnO_2)_{32}(H_2O)_{44}$ (d = 19 Å)

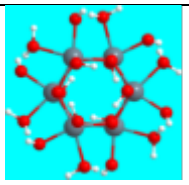

10 , $(H_2SnO_3)_6(H_2O)_6$ (d = 9 Å)

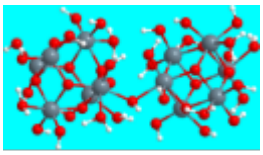

11a , $(H_2SnO_3)_{12}(H_2O)_8$, **1.2**

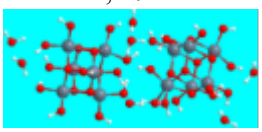

11b , $(H_2SnO_3)_{12}(H_2O)_8$, **6.5**

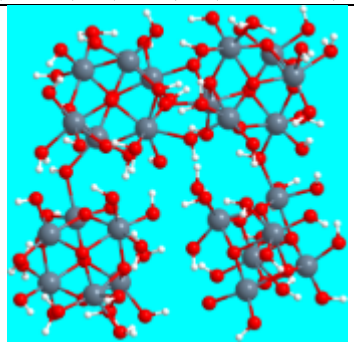

12 , $(H_2SnO_3)_{24}(H_2O)_{16}$, **0.0** (d = 20 Å)

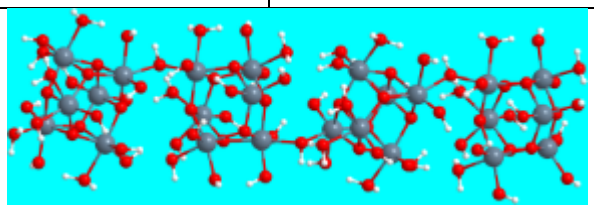

12a , $(H_2SnO_3)_{24}(H_2O)_{16}$, **1.9** (d = 30 Å)

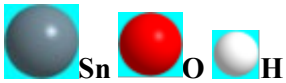

Fig. 1. Zyubina

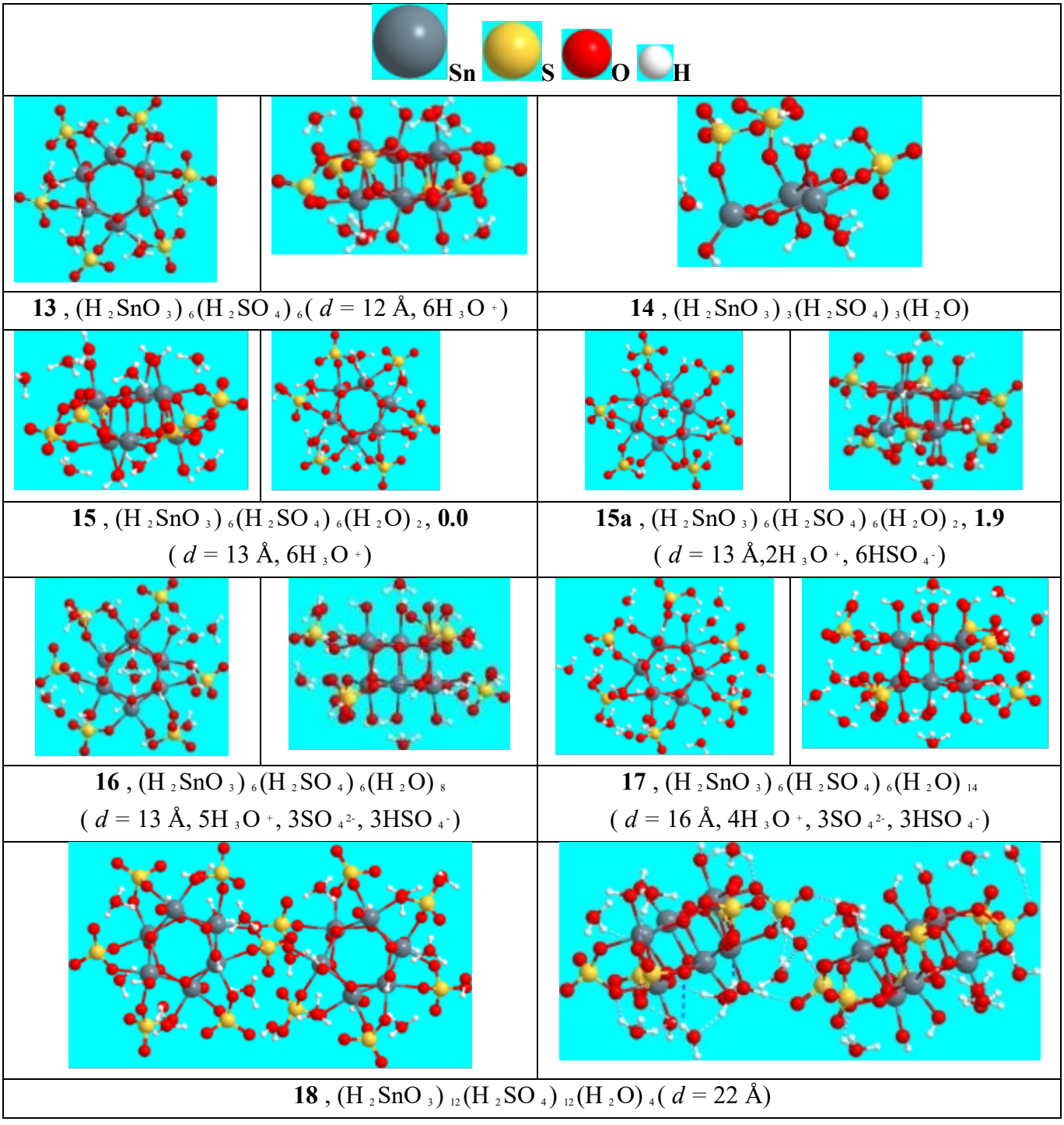

Fig. 2. Zyubina

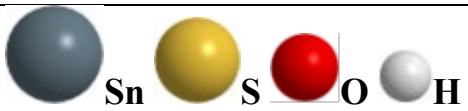

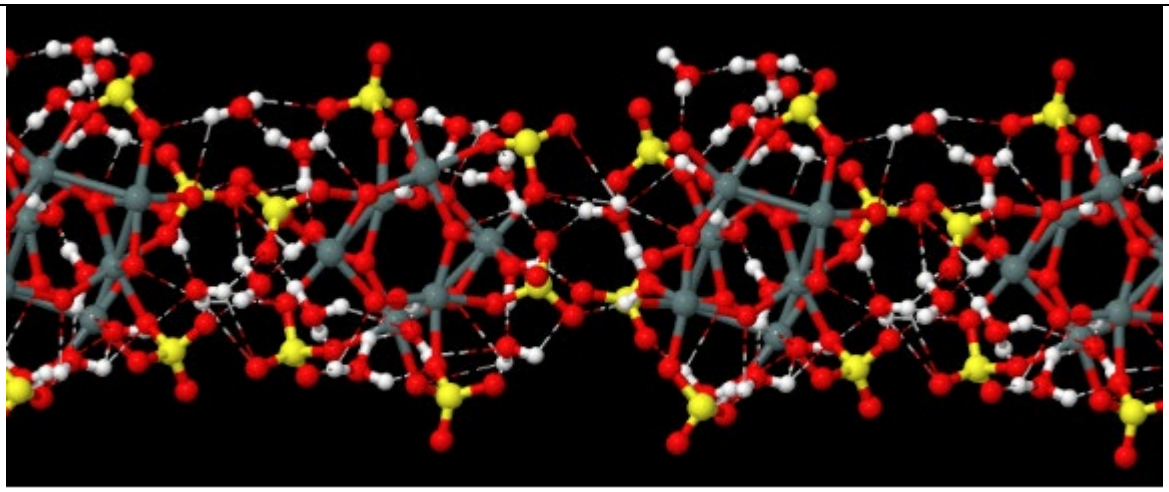

19 , $[(H_2SnO_3)_{12}(H_2SO_4)_{12}(H_2O)_4]$ fiber

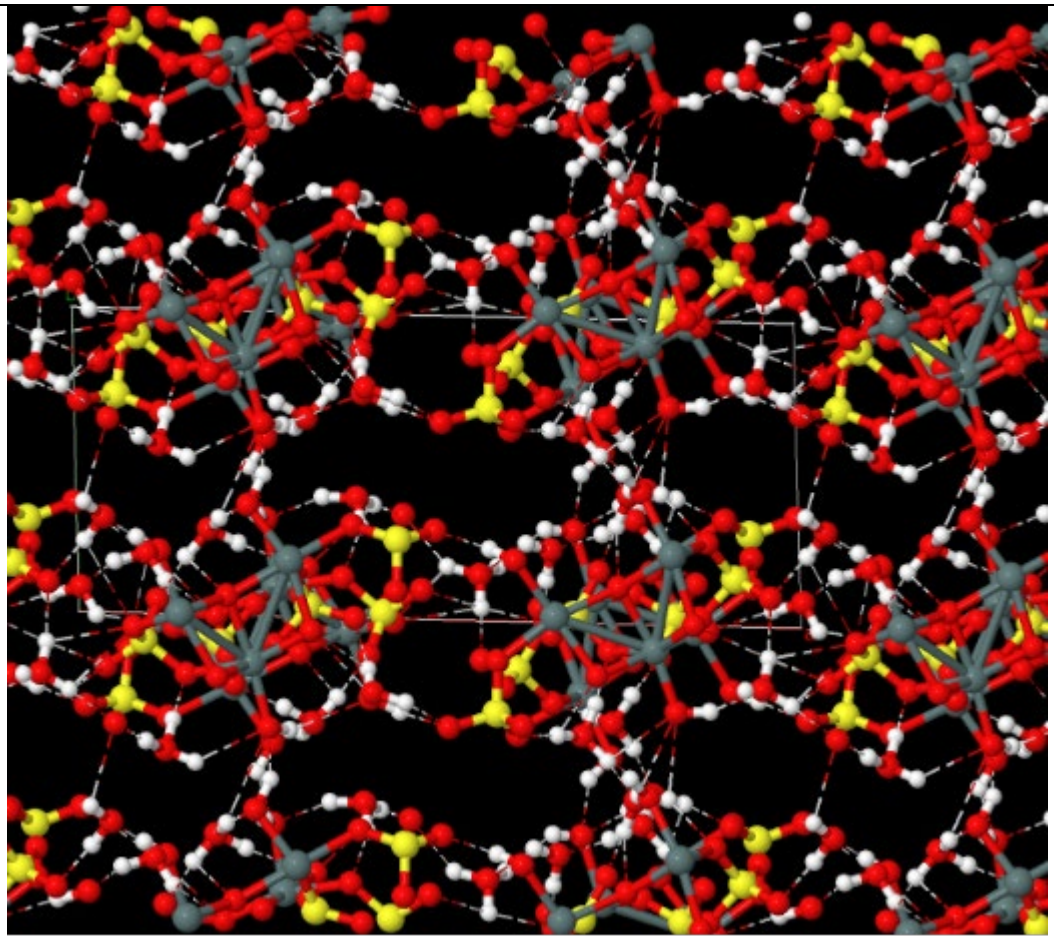

20 , $[(H_2SnO_3)_{12}(H_2SO_4)_{12}(H_2O)_4]$ film

Fig. 3. Zyubina